Title	Nonlinear Dynamic Power Tracking of Low-Power Wind Energy Conversion System
Author(s)	Yang, Y; Mok, KT; Tan, SC; Hui, SYR
Citation	IEEE Transactions on Power Electronics, 2015, v. 30 n. 9, p. 5223-5236
Issued Date	2015
URL	http://hdl.handle.net/10722/209304
Rights	IEEE Transactions on Power Electronics. Copyright © Institute of Electrical and Electronics Engineers.

Nonlinear Dynamic Power Tracking of Low-Power Wind Energy Conversion System

Yun Yang, *Student Member, IEEE*, Kwan-Tat Mok, *Student Member, IEEE*, Siew-Chong Tan, *Senior Member, IEEE*, and S. Y. (Ron) Hui, *Fellow, IEEE*

***Abstract*—This paper addresses the use of variable structure control (i.e., sliding mode (SM) control) for improving the dynamic performance of a low-power wind energy conversion system (WECS) that is connected to a dc grid. The SM control is applied to simultaneously match 1) the maximum power generation of the wind turbine system from the wind with 2) the maximum power injection of the grid-connected power converter into the grid. The amount of energy extractable from a dynamically changing wind using the WECS with SM control is compared with that of classic PI control. Both the simulation and experimental results show that more energy can be harvested with the SM control as compared to the PI control for any dynamically changing or random wind conditions.**

***Index Terms*—Maximum power generation (MPG), maximum power injection (MPI), sliding mode (SM) control, variable structure control, wind energy conversion system (WECS).**

I. Introduction

FOR power systems, 1% of improvement in energy efficiency is a significant achievement. Such significance can be translated to increasing energy harvesting when wide-spread distributed renewable energy generators are installed in the future as a way to drastically reduce greenhouse gas emission. For low-power wind energy conversion systems (WECS), the injected power is small relative to the power capacity of the entire system. All the energy harvested from the wind may be directly injected into the grid without the need for a local energy storage [1]–[3]. This is widely applied in microgrid systems [4]–[6]. Many research efforts on low-power WECS are focused on optimizing the energy conversion, interfacing wind turbines to the grid, and reducing the fatigue load of the mechanical structure [7]–[16]. In particular, maximum power point tracking (MPPT) control plays a crucial role in optimizing the efficiency of the energy conversion [17]–[21]. The MPPT control is applicable not only to the wind power system, but also to photovoltaic and water pumping systems.

Manuscript received June 4, 2014; revised August 25, 2014; accepted September 27, 2014. Date of publication October 15, 2014; date of current version April 15, 2015. This work was supported by the Hong Kong Research Grant Council under Theme-based Research Project: T23-701/14-N. Recommended for publication by Associate Editor L. Chang.

Y. Yang, K.-T. Mok, and S.-C. Tan are with the Department of Electrical & Electronic Engineering, The University of Hong Kong, Hong Kong (e-mail: yangyun@eee.hku.hk; barrymok@connect.hku.hk; sctan@eee.hku.hk).

S. Y. R. Hui is with the Department of Electrical & Electronic Engineering, The University of Hong Kong, Hong Kong and also with the Department of Electrical & Electronic Engineering, Imperial College London, London SW7 2AZ, U.K. (e-mail: ronhui@eee.hku.hk).

Color versions of one or more of the figures in this paper are available online at http://ieeexplore.ieee.org.

Digital Object Identifier 10.1109/TPEL.2014.2363561

It covers an entire class of extremum search algorithms including hill-climbing search [22]–[24], tip-speed ratio control [25]–[27], perturbed and observed [28]–[30], and power signal feedback control [6], etc. Literature review shows that applications of MPPT control in WECS is typically focused on the wind turbine part, which is only concerned with the maximum power generation (MPG) capability, that is, to extract the maximum possible power from the wind. There is a lack of research on the MPPT control of the entire system, covering wind turbine generation, power electronics conversion, and microgrid current injection simultaneously.

In WECS without any energy storage, MPPT of the system is achievable only if the MPG of the wind turbine matches the maximum power injection (MPI) of the load, i.e., a maximum power flow taking place within the system. Moreover, conventional research mainly focuses on the steady-state tracking of the MPPT. In reality, wind is intermittent, and is therefore, a time-varying uncertain parameter. To achieve real-time MPPT control of the system, both the MPG and MPI must be matched dynamically and instantaneously via the control.

This paper addresses the use of variable structure control in the form of sliding mode (SM) control in a low-power WECS to achieve a fast dynamical MPPT of the entire system. SM control is a robust control strategy that guarantees stability against parameter uncertainties, and it gives fast and consistent transient response performance in nonlinear systems that are operated with widely varying input and output conditions. The energy harvesting performance of the SM control will be compared with an optimally tuned proportional-integral (PI) control. Both simulation and experimental verifications are provided.

II. Overview of the System and Analysis of Wind Turbine Characteristics

The schematic diagram of the proposed dc grid-tied low-power WECS system is presented in Fig. 1. The power level of this system is at several kilowatts. It comprises two subsystems, namely the wind turbine system and the power conversion system. The wind turbine system converts the wind energy into ac electrical energy. The function of the power conversion system is to convert the ac electrical voltage to the dc grid voltage level and to inject power to the grid. By applying the MPPT scheme to regulate the torque of the wind turbine via controlling the output voltage E_{rmf} of PMSG, MPG can be achieved. The MPPT controller 1 is required for this purpose. However, it must be emphasized that without a local storage, all power generated must be injected into the grid. If this is not achieved, the power generation will follow the grid-injected power and MPG will not

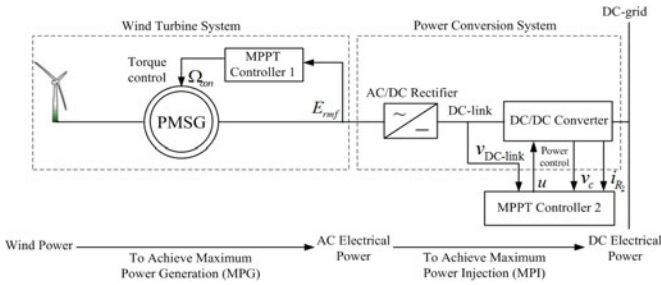

Fig. 1. Overview of a low-power WECS system.

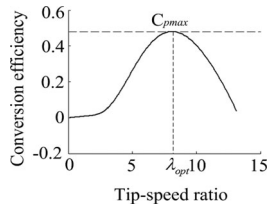

Fig. 2. Wind power coefficient curve of the wind turbine with a constant pitch.

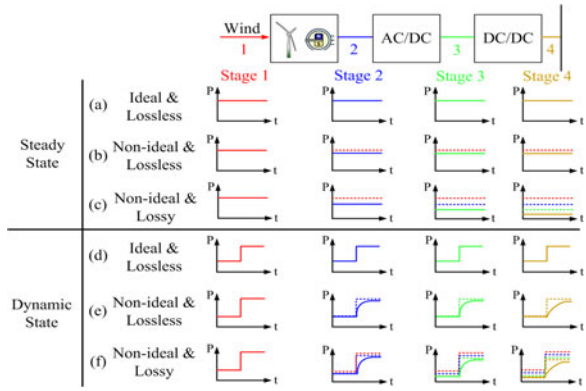

Fig. 3. Power states of the system under different considerations.

be attained even if MPPT control is applied to the wind turbine system. The state of the power conversion system ensuring that the power generated from the wind turbine system with MPG are injected into the grid via the power conversion system will, henceforth, be known as MPI. To achieve MPI, the MPPT control must also be applied to the power conversion system such that its output power injected into the grid matches the MPG. This is achieved via the MPPT controller 2 using state feedback signals of $V_{\mathrm{DC-link}}$, i_{R_2} and v_C. For the wind turbine, the turbine simulated/emulated is a typical 6-m diameter blade for residential use. The PMSG is a three-phase, round rotor ac type generator. For the power conversion part, the ac/dc rectifier is a passive three-phase diode bridge rectifier. The dc/dc converter is a grid-tied buck converter. The variables $V_{\mathrm{DC-link}}$, i_{R_2}, and v_C represent, respectively, the input voltage, the output current, and the output voltage of the buck converter. In this system, the mechanical output power generated by the wind turbine is [6]

$$P_{\mathrm{out}} = \frac{1}{2}\rho S_w v^3 C_p(\beta, \lambda) \tag{1}$$

where ρ is the air density; S_w is the swept area of the wind blade; v is the wind speed; $C_p(\beta, \lambda)$ is the conversion efficiency; β is the pitch angle of the blade; λ is the tip-speed ratio, where $\lambda = \frac{R\omega}{v}$; R is the blade radius; and ω is the angular velocity of the rotating blades. Since the wind power level is low at only a few kilowatts, a constant value of β is adopted [3]. According to [31], $C_p(\beta, \lambda)$ can be expressed as

$$C_p(\lambda) = 0.5176\left(\frac{116}{\lambda_i} - 5\right)e^{\frac{-21}{\lambda_i}} + 0.0068\lambda \tag{2}$$

where $\frac{1}{\lambda_i} = \frac{1}{\lambda} - 0.035$. Then, the mechanical equation of the shaft can be expressed as [32]

$$J\frac{d\Omega}{dt} = T_g - T_e - f\Omega \tag{3}$$

where J and f are, respectively, the total moment of the inertia and the viscous friction coefficient; T_g is the gearbox torque; T_e is the generator torque; and Ω is the mechanical generator speed. By considering the gearbox, the following equation can be obtained

$$G = \frac{\Omega}{\Omega_t} \tag{4}$$

where G is the gear ratio and Ω_t is the rotor speed of the turbine.

As wind speed varies, the optimal value of λ must be maintained to ensure that the value of $C_p(\lambda)$ is at its maximum $C_{p\max}$. Since $\lambda = \frac{R\omega}{v}$, $\frac{\Omega_t}{v}$ should be constant. Thus, Ω_t is chosen to trace the variation of the wind speed. The wind power coefficient curve with a constant pitch ($\beta = 0$) can be plotted as shown in Fig. 2.

III. Nonideal Dynamic Power Extraction

A. Overview of Power Flow of the Entire System

The operation of the WECS can be classified into four stages as shown in Fig. 3. Stage 1 represents the maximum available power that the wind turbine system can electrically harvest from the wind. Stage 2 represents the actual electrical power extracted by the wind turbine system in ac form. Stage 3 is the electrical power after rectification from ac voltage to dc voltage by the ac/dc rectifier. Stage 4 represents the final electrical power of the system after dc/dc power conversion and that being injected into the grid.

In the ideal condition of perfect MPPT tracking and assuming lossless power conversion [see Fig. 3(a)], the power in Stage 2 will be equivalent to that in Stage 1. This indicates that all available wind power is harvested, thereby achieving MPG. Here, all the harvested power are injected into the grid through the ac/dc rectifier and the dc/dc converter, thereby achieving MPI. Therefore, the power level of Stages 1–4 are equivalent. The power injected into the grid perfectly matches the power generated by the wind turbine. However, in reality, the nonideal conditions of imperfect MPPT control by either the wind turbine system and/or the power conversion system, and their power losses, need to be considered. In the case of a nonideal MPPT and lossless system [see Fig. 3(b)], the inability of either the wind turbine system or the power conversion system in achieving

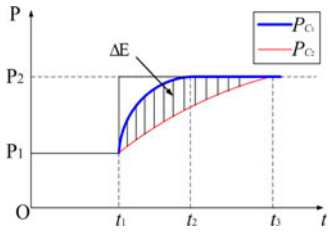

Fig. 4. Extracted power from the wind turbine system during transient for different controllers, i.e., P_{C_1} (fast controller C_1) and P_{C_2} (slow controller C_2).

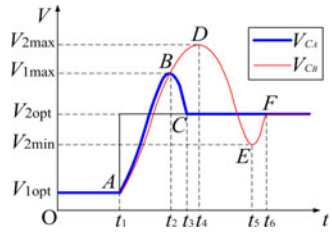

Fig. 5. Analysis of input voltage $V_{\mathrm{DC-link}}$ of the dc/dc converter during a step transient for different controllers.

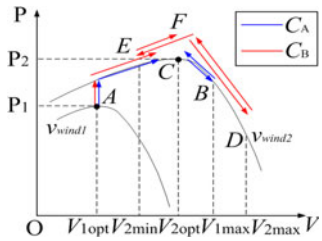

Fig. 6. Output power versus dc-link voltage.

perfect MPPT will lead to a suboptimal MPG or a suboptimal MPI. Unextractable power is wasted. In either case, the power flow of the overall system will be limited by the lower of the two. Therefore, the power in Stages 2–4 are equivalent and are lower than that of Stage 1. Next, by considering the power loss in each stage, the actual power present in Stages 2 to 4 will be similar to that illustrated in Fig. 3(c) (solid line representing the actual power of each stage).

Similar arguments can be applied to the three cases under the dynamic situations, as illustrated in Fig. 3(d)–(f). With both the wind turbine and power conversion systems possessing inertia and requiring time for controllers to react for any change in wind power, the reality is that there will be a transient period when there is a mismatch between the desired MPG and the desired MPI. In such a situation [see Fig. 3(e)], in the event of a power change in Stage 1, the power in Stage 2 will reach the new steady state after some time. Furthermore, the power flow will be limited by the lower of the suboptimal MPG and suboptimal MPI, which makes the new steady-state power lower than the ideal one. Power in Stages 2–4 are equivalent. It is, therefore, clear that fast and accurate controllers should be employed to regulate the actual power flow closely to the perfect maximum power flow condition, both in transient and in steady state.

B. MPPT of Wind Turbine System

Consider the use of a fast controller C_1 and a slower controller C_2 in the wind turbine system. In the extreme case of a step change of wind power from P_1 and P_2, the output power extractable from the wind would be different for the two controllers, as illustrated in Fig. 4. Here, the fast controller C_1, which arrives at the MPG condition faster and more accurately, will allow the system to harvest more electrical power from the wind energy.

From Fig. 4, the ideal amount of wind energy that can be harvested during the transient period from t_1 to t_3 is

$$E_{\mathrm{ideal}} = \int_{t_1}^{t_3} P_2 dt = P_2 \left(t_3 - t_1\right). \tag{5}$$

For the fast controller C_1, the energy harvested for the same period is

$$\begin{aligned} E_{C_1} &= \int_{t_1}^{t_2} P_{C_1}\left(t\right) dt + \int_{t_2}^{t_3} P_2 dt \\ &= \int_{t_1}^{t_2} P_{C_1}\left(t\right) dt + P_2\left(t_3 - t_2\right). \end{aligned} \tag{6}$$

The amount of energy harvested by the system using the controller C_2 is

$$E_{C_2} = \int_{t_1}^{t_3} P_{C_2}\left(t\right) dt. \tag{7}$$

It is obvious that

$$E_{\mathrm{ideal}} > E_{C_1} > E_{C_2}. \tag{8}$$

The extra energy harvested by the system with C_1 is

$$\begin{aligned} \Delta E = &\int_{t_1}^{t_2} \left(P_{C_1}\left(t\right) - P_{C_2}\left(t\right)\right) dt \\ &+ \int_{t_2}^{t_3} \left(P_2 - P_{C_2}\left(t\right)\right) dt > 0 \end{aligned} \tag{9}$$

where $\Delta E = E_{C_1} - E_{C_2}$, as represented by the shaded area given in Fig. 4.

C. MPPT of Power Conversion System

Without energy storage, any change of the wind power will cause a corresponding change in the input power of the ac/dc converter and its output dc voltage $V_{\mathrm{DC-link}}$, i.e., input voltage of the dc/dc converter. It is necessary to use a fast controller in the dc/dc converter for achieving MPI. A fast controller C_A and a slow controller C_B will give different transient performance which affects $V_{\mathrm{DC-link}}$, as illustrated in Figs. 5 and Fig. 6 shows a typical *P–V* (output power versus dc-link voltage) curve of this system for two wind speeds. The movements of the trajectory for searching the maximum power point (MPP) of the two controllers are illustrated in Fig. 5.

Initially, with a wind speed of v_{wind1}, the power conversion system (for both C_A and C_B controllers) is operating optimally at the MPP A with a power of P_1 and dc-link voltage of $V_{1\mathrm{opt}}$ (see Figs. 5 and 6. With a sudden change of the wind speed to v_{wind2}, there is a corresponding change of the available wind

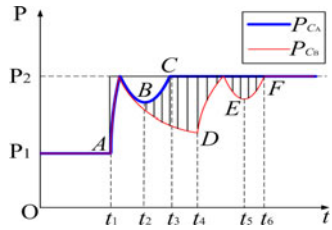

Fig. 7. Output power during transient for different controllers, namely, P_{C_A} (fast controller C_A) and P_{C_B} (slow controller C_B).

power from P_1 to P_2 at the input of the ac/dc converter in the power conversion system. However, since the output of the ac/dc passive rectifier comprises a capacitor, which requires time to charge, the change of the dc-link voltage cannot be instantaneously changed with respect to the change in its input power. Thus, the dc-link voltage remains at $V_{1\text{opt}}$ even though the voltage operating point for achieving the maximum power is $V_{2\text{opt}}$ at point C of the curve. As shown in Fig. 5, it takes some time before the power flow and dc-link voltage of the dc/dc converter can be controlled to reach $V_{2\text{opt}}$. With C_A, the dc-link voltage changes from point A at t_1, to point B at t_2, and then, finally being controlled to point C at t_3. Fig. 6 explains the geometric relationship between the output power and the dc-link voltage of the system that is controlled by a fast controller C_A and a slow controller C_B. After a sudden wind change from v_{wind1} to v_{wind2}, the fast controller C_A seeks the new MPP with a small dc-link voltage overshoot to point B, and then, back to the MPP C in Fig. 6. For the slow controller C_B, the dc-link voltage overshoots to point D, then to point E, and finally, to the MMP F. Mapping Fig. 5 into Fig. 6, the corresponding output power waveform of the power conversion system with C_A can be obtained, and is shown in Fig. 7. Similar power waveform can be obtained for the system with C_B by considering the dc-link voltage waveform of C_B in Fig. 5. From Fig. 7, it can be seen that the dc/dc converter with C_A reaches the steady-state P_2 earlier than that with C_B. Therefore, within the transient period from t_1 to t_6, more energy is transferred from the rectifier to the power grid with controller C_A. The difference in the energy transferred between C_A and C_B is represented by the shaded area in Fig. 7.

IV. SM Control Design for the System

The MPPT computation technique adopted in this paper is the tip-speed ratio control. The SM control is used to perform the MPPT control of both the wind turbine system and the power conversion system. The control design is performed individually on the respective systems before they are being merged into a single system. The system performance will be compared with that of the conventional PI controllers.

A. SM Control Design of Wind Turbine System

According to (4) and the expression of the tip-speed ratio, the reference of the mechanical generator speed can be derived as

$$\Omega_{\text{ref}} = \frac{\lambda_{\text{opt}} v G}{R}. \tag{10}$$

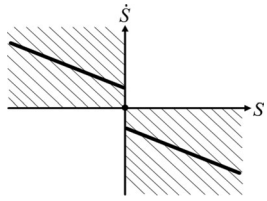

Fig. 8. SM dynamics for sliding surface.

The goal is to control the mechanical generator speed to run at this reference speed such that the tip-speed ratio is optimum, thereby leading to the generation of the maximum electrical output power. According to [33], the sliding surface can be chosen as

$$S = \dot{\Omega}_{\text{ref}} - \dot{\Omega} + c \cdot (\Omega_{\text{ref}} - \Omega) \tag{11}$$

where c is a tuning factor. By substituting (3) and (10) into the time derivative of (11) gives

$$\dot{S} = \left(\frac{f^2}{J^2} + \frac{c \cdot f}{J}\right) S + \left(\frac{f}{J^2} + \frac{c}{J}\right)(T_e - T_g) + \ddot{\Omega}_{\text{ref}} + c \cdot \dot{\Omega}_{\text{ref}} - \left(\frac{f^2}{J^2} + \frac{c \cdot f}{J}\right)\Omega_{\text{ref}}. \tag{12}$$

To satisfy the Lyapunov stability criteria $S \cdot \frac{dS}{dt} < 0$ [33], (12) must be located in the shaded zones in Fig. 8.

A piecewise function form of (12) can meet such a requirement satisfying concurrently all three conditions of SM operation, i.e., hitting, existence, and stability conditions. With this, the mathematical expression of the SM controller for the wind turbine system can be obtained as

$$\Omega_{\text{con}} = f\Omega_{\text{ref}} - \alpha_1 \ddot{\Omega}_{\text{ref}} - \left(J - \frac{f}{J}\alpha_1\right)\dot{\Omega}_{\text{ref}} - \alpha_2 \text{sgn}(\Omega_{\text{ref}} - \Omega) \tag{13}$$

where $\text{sgn}(.)$ is a signum function, and $\alpha_1 = \frac{J^2}{c \cdot J + f}$ and α_2 are the tuning factors. The detailed SM control block diagram is given in Fig. 9(a).

In the case of applying PI control to the wind turbine system, the mathematical expression of the PI controller will be

$$\Omega_{\text{con}} = K_p (\Omega_{\text{ref}} - \Omega) + K_i \int_0^t (\Omega_{\text{ref}} - \Omega) dt \tag{14}$$

where K_p is the proportional gain and K_i is the integral gain. The detailed PI control block diagram is given in Fig. 9(b).

B. SM Control Design of Power Conversion System

Fig. 10 shows the topology of the grid-tied dc/dc buck converter used in this system. With a widely varying input voltage and input power, it can be equivalently considered as a general buck converter with widely varying input voltage and load, which can be well regulated by the SM controller [34]. The mathematical expression of the buck converter with the SM

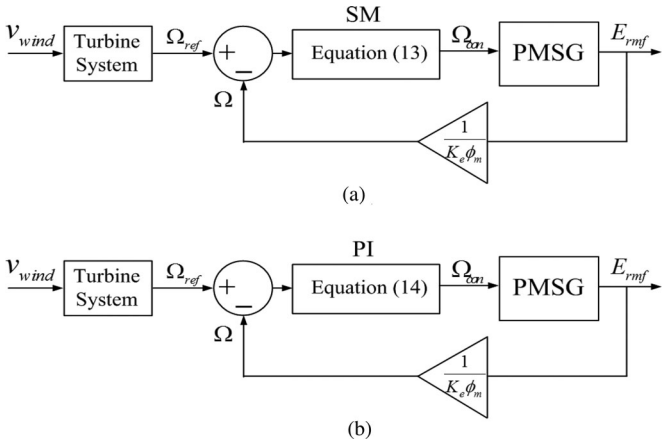

Fig. 9. Detailed (a) SM and (b) PI control block diagram of the wind turbine system that will be compared in this study.

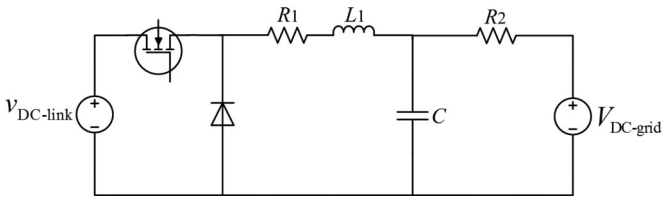

Fig. 10. Grid-tied dc/dc buck converter topology.

controller is

$$\begin{cases} v_{\mathrm{DC-link}} \cdot u = L_1 \dfrac{di_{L_1}}{dt} + R_1 i_{L_1} + v_c \\ V_{\mathrm{DC-grid}} = -R_2 i_{L1} + R_2 C \dfrac{dv_c}{dt} + v_c. \end{cases} \tag{15}$$

The sliding surface is selected as

$$S(\mathbf{x}, t) = \sum_{i=1}^{3} \alpha_i x_i(t) \tag{16}$$

where α_i represents the sliding coefficients and $x_i(t) \in \mathbf{x}(t)$. The control variables are

$$\mathbf{x} = \begin{bmatrix} x_1 \\ x_2 \\ x_3 \end{bmatrix} = \begin{bmatrix} v_{\mathrm{ref}} - \beta v_c \\ \dfrac{d(v_{\mathrm{ref}} - \beta v_c)}{dt} \\ \int (v_{\mathrm{ref}} - \beta v_c) dt \end{bmatrix}. \tag{17}$$

The SM control strategy is based on the PWM-based SM controller scheme presented in [34] and can be determined as

$$v_{\mathrm{con}} = K_1 i_C + K_2 v_c + K_3 \tag{18}$$

and

$$|v_{\mathrm{ramp}}| = \beta v_{\mathrm{DC-link}} \tag{19}$$

where $K_1 = -\frac{\alpha_1 \beta L_1}{\alpha_2} + \beta \left(\frac{L_1}{R_2 C} + R_1 \right)$, $K_2 = -\frac{\alpha_3 \beta L_1 C}{\alpha_2} + \beta \left(\frac{R_1}{R_2} + 1 \right)$, and $K_3 = -\frac{\beta R_1}{R_2} V_{\mathrm{DC-grid}} + \frac{\alpha_3}{\alpha_2} L_1 C \left(\frac{P_{\mathrm{ref}}(V_{\mathrm{DC-link}})}{V_{\mathrm{DC-grid}}} R_2 + V_{\mathrm{DC-grid}} \right)$. Here, v_{con} is the control signal, v_{ramp} is the ramp signal for PWM modulation, and $|v_{\mathrm{ramp}}|$ is the amplitude of v_{ramp}. The coefficients are selected to satisfy the hitting, existence, and stability conditions of SM operation [34].

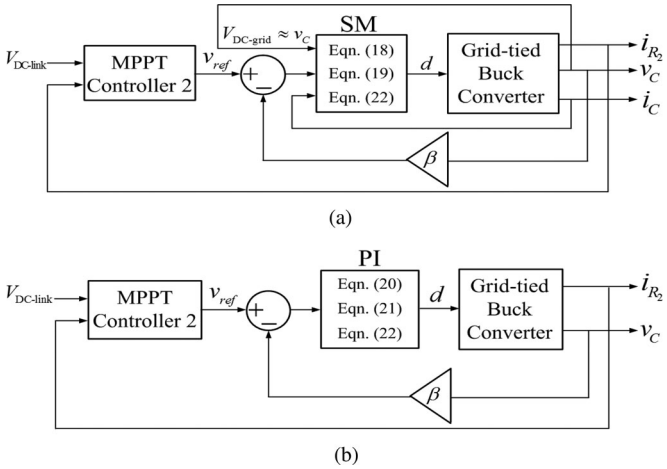

Fig. 11. Detailed (a) SM and (b) PI control block diagrams of power conversion system.

TABLE I
SPECIFICATIONS OF THE WIND TURBINE SYSTEM

Parameters	Values
Radius of Rotor	3 m
Number of blades	3
Density of air	1.225 $\mathrm{kg/m^3}$
Gear ratio	5
Friction coefficient	0.002 $\mathrm{N \cdot m/s}$
Turbine inertia	0.2 $\mathrm{kg \cdot m^2}$

In the case of applying PI control to the power conversion system, the expression of the PI controller is

$$v_{\mathrm{con}} = K_p \left(v_{\mathrm{ref}} - \beta v_c \right) + K_i \int_0^t (v_{\mathrm{ref}} - \beta v_c) dt \tag{20}$$

and

$$|v_{\mathrm{ramp}}| = \text{constant} \tag{21}$$

where K_p is the proportional gain and K_i is the integral gain. Then, the duty cycle d of each of the controller can be derived using the same equation

$$d = \frac{v_{\mathrm{con}}}{|v_{\mathrm{ramp}}|}. \tag{22}$$

The detailed SM and PI control block diagrams are given in Fig. 11(a) and (b), respectively.

V. SIMULATION RESULTS

The parameters of the wind turbine system and the power conversion system used in the simulation are given in Tables I and II, respectively. Generally, for a low-power wind system,

TABLE II
SPECIFICATION OF THE POWER CONVERTER SYSTEM

Parameters	Values	Parameters	Values
L_1	1.3 mH	R_1	0.2 Ω
R_2	0.2 Ω	C	20 μF
$V_{\mathrm{DC-grid}}$	100 V	I_{R_2}	5.28 A ∼ 42.21 A
$v_{\mathrm{DC-link}}$	200 V ∼ 700 V	$I_{\mathrm{DC-link\_max}}$	10 A

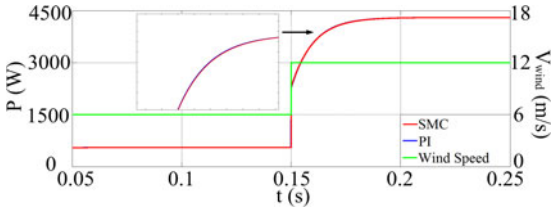

Fig. 12. Comparison of turbine-generated output power using PI control and SM control for full range condition.

the typical maximum operating wind speed is $v_{\mathrm{wind}} = 12\ \mathrm{m/s}$ and the operating minimum wind speed is $v_{\mathrm{wind}} = 6\ \mathrm{m/s}$ [6]. Therefore, a full power range of the wind speed changing from 6 to 12 m/s is applied for the optimal tuning of both the PI controllers and the SM controllers to achieve the best possible performance for this step change. In this study, the PI control of both the wind turbine system and the power conversion system are empirically tuned using the well-known Ziegler–Nichols tuning method. The SM control for the wind turbine system is tuned by trial-and-error. The SM control for the power conversion part is designed using SM design guidelines provided in [34].

A. PI Control Versus SM Control of Wind Turbine System for Achieving MPG

For the wind turbine system, the values of $K_p = 21.524$ and $K_i = 0.178$ are adopted in the PI control and the values of $\alpha_1 = 0.01$ and $\alpha_2 = 100$ are chosen as the coefficients of the SM controller. These two controllers are tuned to give the same optimal performance in power extraction for a step change from $v_{\mathrm{wind}} = 6\ \mathrm{m/s}$ to $v_{\mathrm{wind}} = 12\ \mathrm{m/s}$. The simulated results are given in Fig. 12. However, with a change in the dynamic operating condition of the wind speed from its original condition, the results are different. The SM controller performs better in generating more power during the transient period in all situations than the PI controller, as shown in Fig. 13. This demonstrates the strength of SM control in handling dynamically varying operating conditions in nonlinear systems, which in this case, is to respond quickly to tracking the MPPT point for MPG when wind speed varies. With the SM control always reaching the desired maximum power conversion coefficient faster than the PI control when wind speed changes (see in Fig. 14), the energy harvesting with the SM controller (i.e., E_{SM}) is better than that with the PI controller (i.e., E_{PI}), as shown in Fig. 15. This is expected and is in full agreement with the theoretical discussion given in Section III

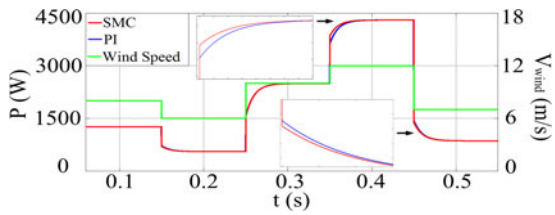

Fig. 13. Comparison of turbine-generated output power using PI control and SM control for various conditions of wind-speed step change.

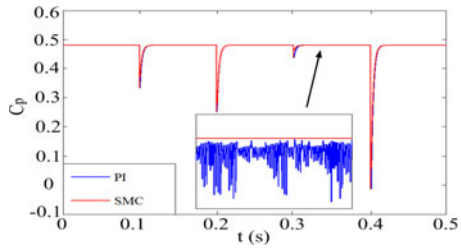

Fig. 14. Power conversion coefficient with PI control and SM control.

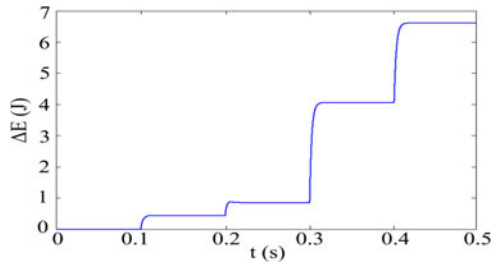

Fig. 15. Difference of energy acquired from the wind between the SM control (E_{SM}) and PI (E_{PI}) control, where $\Delta E(\mathrm{J}) = \mathrm{E_{SM}} - \mathrm{E_{PI}}$.

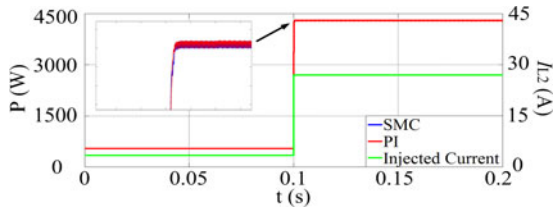

Fig. 16. Output power response of buck converter with PI control and SM control for full injected current range.

B. PI Control Versus SM Control of the Power Conversion System for Achieving MPI

The same procedure is adopted for the design of the power conversion system. Full power range of the output current changing from 5.28 to 42.21 A is applied for the optimal tuning of both the PI and SM controller. Here, for the PI control, $K_p = 0.5$ and $K_i = 120$. For the SM control, $K_1 = 0.0153$, $K_2 = 7.2$, and $\beta = 0.025$. As shown in Fig. 16, both controllers have similar transient performance. Then, a step change of the injected current of the grid-tied dc/dc converter from 12.51 A to 5.28 A to 24.43 A to 42.21 A to 8.38 A is performed to compare the performance of the two controllers, which is given in Fig. 17.

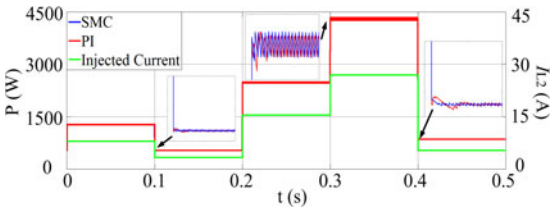

Fig. 17. Output power response of buck converter with PI control and SM control for varying injected current step changes.

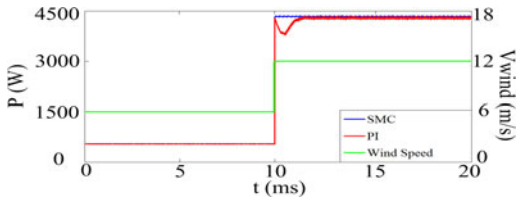

Fig. 18. Overall system performances with PI control and SM control for full range operating condition.

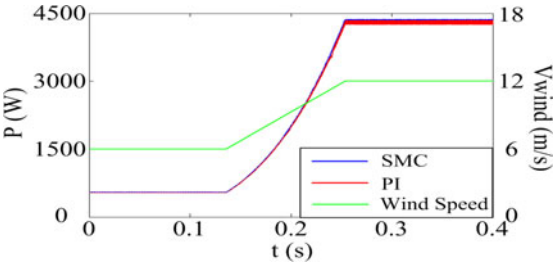

Fig. 19. Overall system performances with PI control and SM control for full range operating condition with consideration to the 100 ms wind-speed change time constant.

For all these conditions, a faster transient performance with less overshoot is achievable with the SM control.

C. Overall System Controlled by PI Controller and SM Controller

With the PI controllers and SM controllers optimally tuned for the respective wind turbine system and the power conversion system, both these systems are then connected together for operation. It is found that the optimally tuned system with PI control is no longer optimal when operated as a whole system for wind speed changing from 6 to 12 m/s as compared to the system with SM control, which still performs optimally, as illustrated in Fig. 18. In real world, the wind velocity itself may take at least one hundred milliseconds to actually change from 6 to 12 m/s. Fig. 19 shows the results of the system under the two controllers with such a wind condition. Figs. 20 and 21 show the corresponding energy acquisition by both controllers and the difference in their energy acquisition. The results show that 0.89% more energy can be harvested with the SM controller.

Also, wind speed changing from 8 m/s to 6 m/s to 10 m/s to 12 m/s to 7 m/s at every 0.1 s are applied. The waveforms provided in Fig. 22 show that the optimally tuned PI controllers are

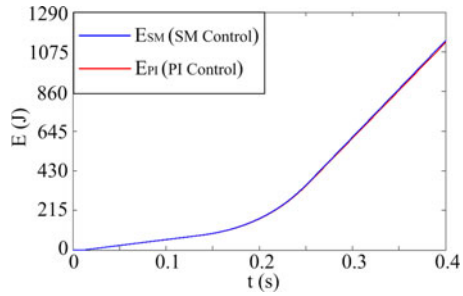

Fig. 20. Energy acquisition by the SM control and the PI control for the overall system with consideration to the 100-ms wind-speed change time constant.

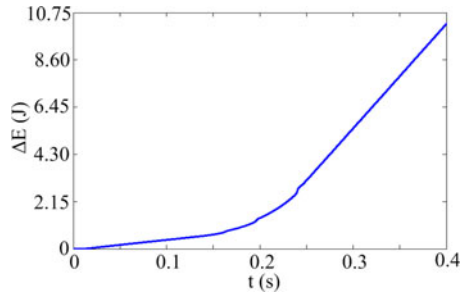

Fig. 21. Corresponding difference of energy acquired between the SM control (E_{SM}) and PI (E_{PI}) control, where $\Delta E(\mathrm{J}) = \mathrm{E_{SM}} - \mathrm{E_{PI}}$.

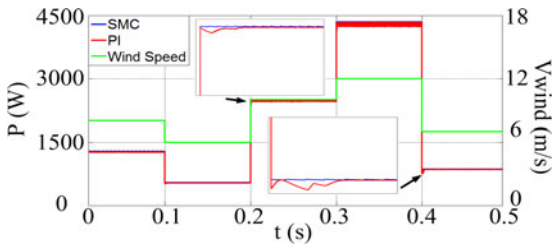

Fig. 22. Overall system performances of the PI control and the SM control for varying wind-speed step change conditions.

incapable of tracking the desired parameters of such a nonlinearly cascaded system with widely varied operating conditions. Its transient performance is poor as compared to that achievable with SM control, which gives a robust performance for all changes. With a wind speed that changes repeatedly from 8 m/s to 6 m/s to 10 m/s to 12 m/s to 7 m/s over a period of 5 min, the energy acquisition for the overall system by both SM and PI controllers and the difference in their energy acquisition are simulated and are, respectively, shown in Figs. 23 and 24. The results show that 3% more energy can be harvested from the system with the SM controller. This validates our analysis given in Section III.

Finally, under the stochastic wind conditions from 6 m/s to 12 m/s, power comparisons for two controllers are given in Figs. 25. Fig. 26 shows the energy acquisition by two controllers and Fig. 27 shows the difference in energy acquisition. The results show that under such a stochastic wind, 2.1% more energy can be harvested with the SM controller than PI the controller.

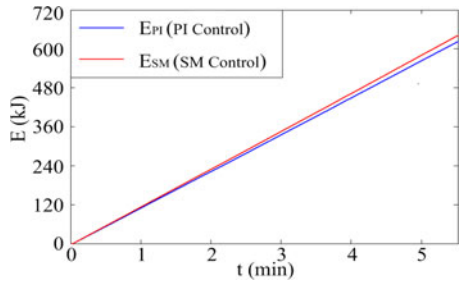

Fig. 23. Energy acquisition by the SM control and the PI control for the overall system.

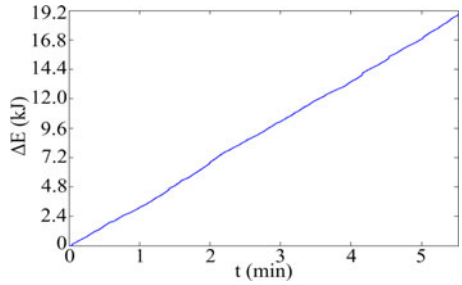

Fig. 24. Difference of energy acquired from the wind between the SM control (E_{SM}) and PI (E_{PI}) control, where $\Delta E(\mathrm{J}) = \mathrm{E_{SM}} - \mathrm{E_{PI}}$.

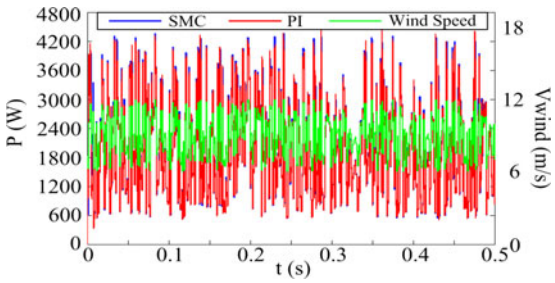

Fig. 25. Overall system performances for the PI control and the SM control for full range operating condition with stochastic wind.

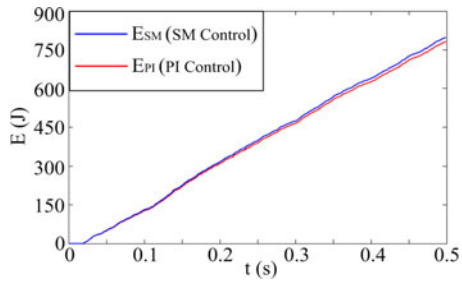

Fig. 26. Energy acquisition by the SM control and the PI control for the overall system with stochastic wind.

VI. Experimental Results

The comparison of the experimental performance of the SM and PI controllers are carried out for the MPG part, the MPI part, and the MPPT of the whole system. For the MPG part, a Triphase PM15F80C is used to emulate the wind turbine system. The characteristic of the WECS is programmed into the Triphase PM15F80C. It should, however, be noted that in the practical tests, the wind speed range in the profile is limited from 6.6 to 7.9 m/s, which corresponds to the limited output ac voltage of the Triphase PM15F80C from 180 to 220 V. Such range is much smaller than that used in the simulation study (i.e., 6 to 12 m/s). Nevertheless, it will be shown that noticeable difference in extra energy harvesting can be achieved with the SM control. The waveforms of the output ac voltage, output ac current, and output active power of the system under the PI and SM control are depicted, respectively, in Fig. 28(a) and (b). Here, both the PI and SM controllers are optimally tuned for the best performance under this wind speed change condition. For the SM controller, the average output real power over two transient cycles is 431.6 W and for the PI controller, the power is 430.7 W. The difference in their power extraction capability is very small.

Various experiments are then performed with the wind speed being changed from 1) 7.9 to 6.6 m/s, 2) 6.6 to 7.3 m/s, and 3) 7.3 to 6.6 m/s. The corresponding results are presented in Figs. 29–31, which show a maximum power difference of 6.9 W between the two controllers for wind speed change from

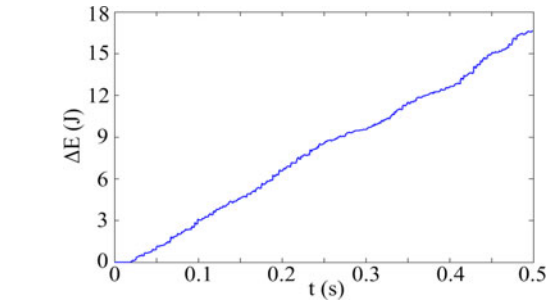

Fig. 27. Difference of energy acquired from the stochastic wind between the SM control (E_{SM}) and PI (E_{PI}) control, where $\Delta E(\mathrm{J}) = \mathrm{E_{SM}} - \mathrm{E_{PI}}$.

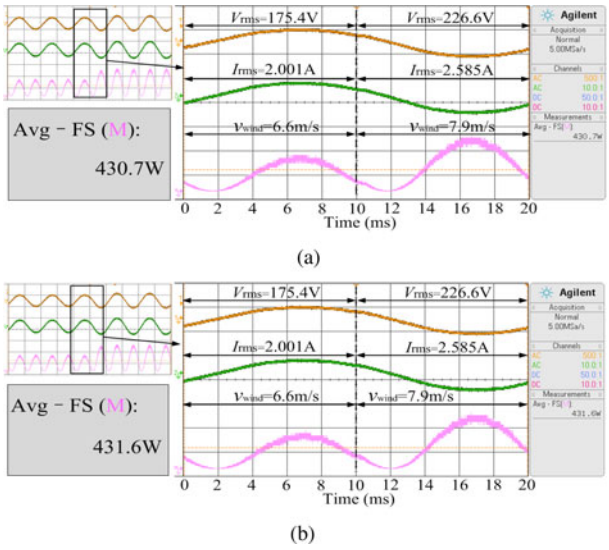

Fig. 28. Experimental results of the output ac voltage, output current, and MPG of wind turbine system corresponding to the wind speed changing from 6.6 to 7.9 m/s under (a) PI control and (b) SM control.

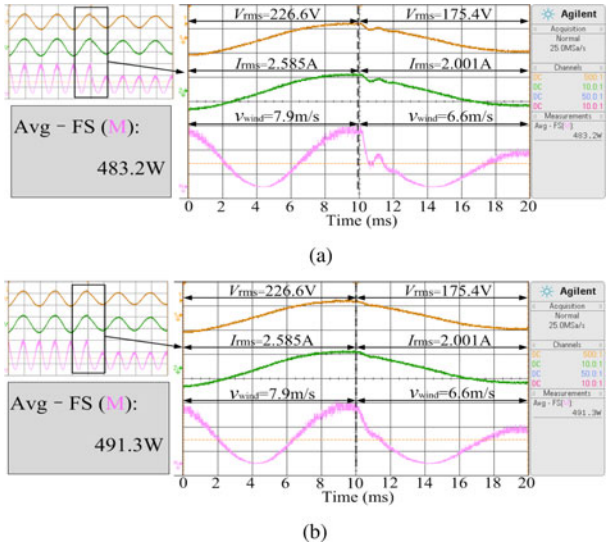

Fig. 29. Experimental results of the output ac voltage, output current, and MPG of wind turbine system corresponding to the wind speed changing from 7.9 to 6.6 m/s under (a) PI control and (b) SM control.

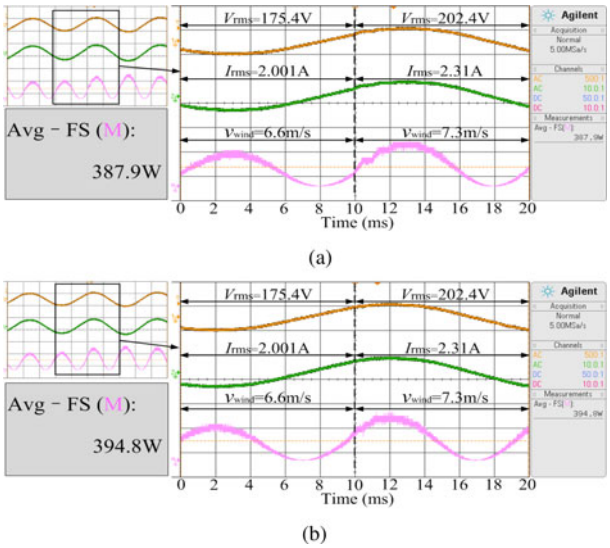

Fig. 30. Experimental results of the output ac voltage, output current, and MPG of the wind turbine system corresponding to the wind speed changing from 6.6 to 7.3 m/s under (a) PI control and (b) SM control.

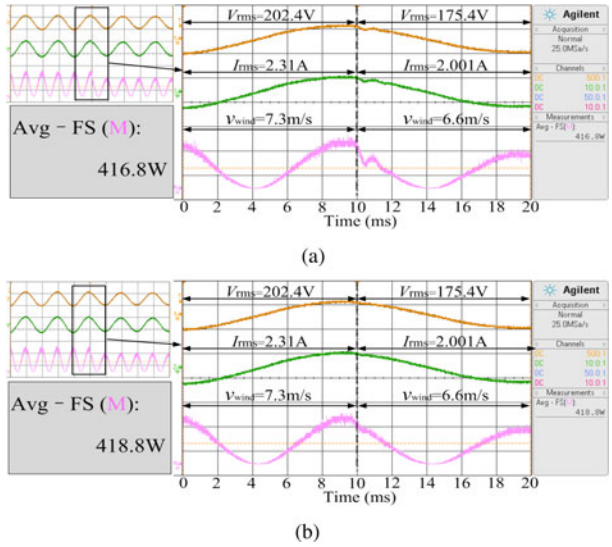

Fig. 31. Experimental results of the output ac voltage, output current, and MPG of wind turbine system corresponding to the wind speed changing from 7.3 to 6.6 m/s under (a) PI control and (b) SM control.

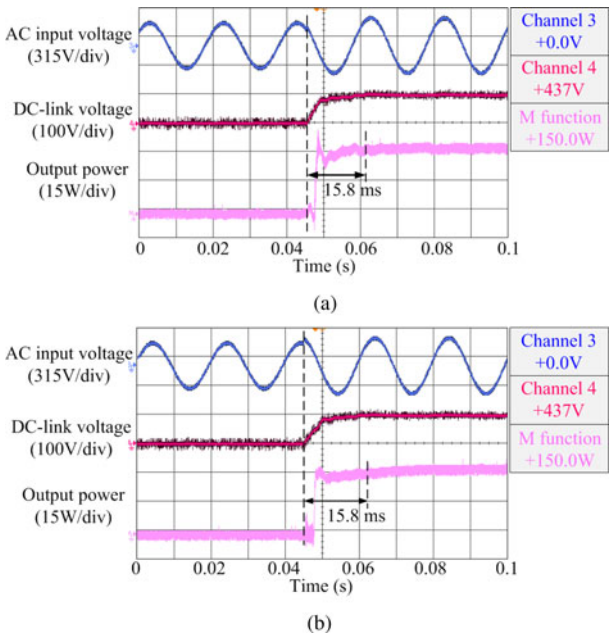

Fig. 32. Experimental results of the dc-link voltage and output power corresponding to the input ac voltage changing from 180 to 220 V under (a) PI control and (b) SM control.

6.6 to 7.3 m/s (see Fig. 30). Even though the wind speed changes are restricted by the hardware, these results consistently indicate that the WECS with SM control can harvest more energy than the PI controller. The difference in their power extraction capability is noticeable.

For the MPI part, a California Instrument CSW 5550 three-phase variable ac power supply is used to emulate the wind turbine system. Here, the output voltage of CSW 5550 will fluctuate according to the wind power variation. The power conversion system comprising an ac/dc rectifier and a dc/dc converter is set up using a Triphase PM5F03R system. For the dc/dc converter, only one leg of the three-legged full bridge dc/dc converter of the Triphase System is used, which is equivalently a buck converter.

In the experiment, the rms of the output ac voltage of the CSW 5550 is changed from 180 to 220 V to simulate a step change in wind energy. The waveforms of the corresponding dc-link voltage from the rectifier and the output power of the dc/dc converter that is regulated by, respectively, the PI and SM controllers, are depicted in Fig. 32(a) and (b). Both the PI and SM controllers are optimally tuned for a similar settling time of 15.8 ms.

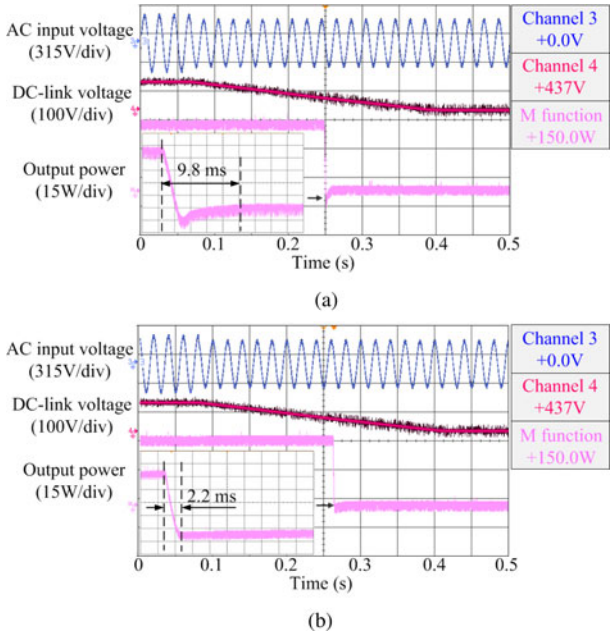

Fig. 33. Experimental results of the dc-link voltage and output power corresponding to the input ac voltage changing from 220 to 180 V under (a) PI control and (b) SM control.

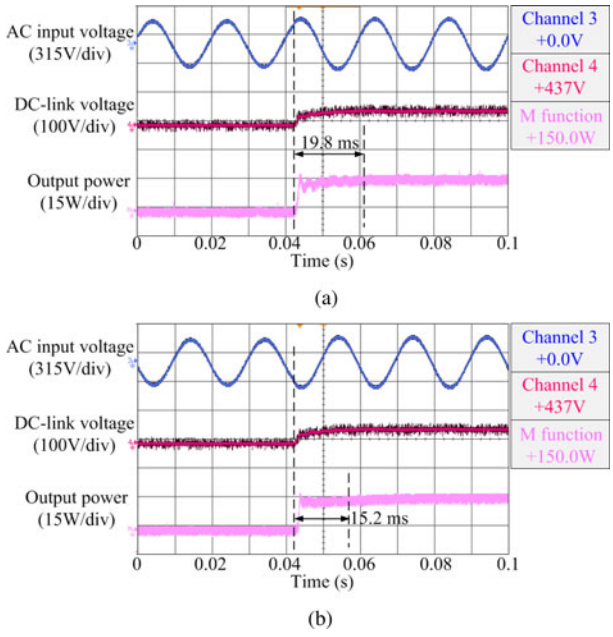

Fig. 34. Experimental results of the dc-link voltage and output power corresponding to the input ac voltage changing from 180 to 200 V under (a) PI control and (b) SM control.

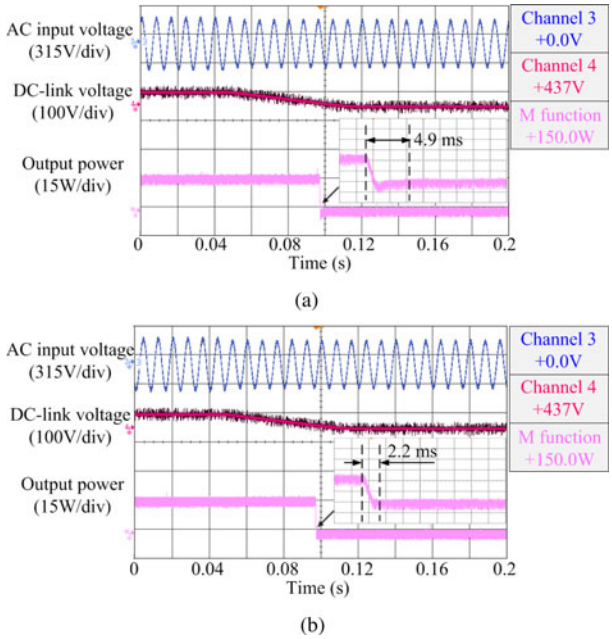

Fig. 35. Experimental results of the dc-link voltage and output power corresponding to the input ac voltage changing from 200 to 180 V under (a) PI control and (b) SM control.

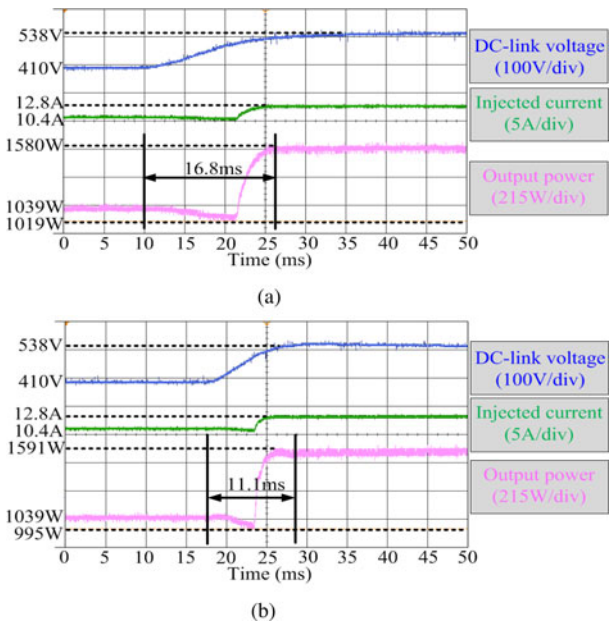

Fig. 36. Experimental results of the dc-link voltage, injected current, and output power of the whole system corresponding to the wind speed changing from 6.6 to 7.9 m/s under (a) PI control and (b) SM control.

Various experiments are then performed with the ac voltage being changed from 1) 220 to 180 V, 2) 180 to 200 V, and 3) 200 to 180 V. The corresponding results are presented in Figs. 33–35. From the results, the WECS with SM control can reach the optimal steady-state point much faster than the PI control.

With that, the MPG and MPI parts are combined into a whole system. A Triphase PM15F80C inverter is used to emulate the wind turbine system and a Triphase PM5F03R inverter is used for the power conversion system. Both the PI and SM controllers are kept their original values as in the MPG and MPI parts. From Fig. 36(a) and (b), the SM controller takes 11.1 ms to reach steady state, while the PI controller takes about 16.8 ms. (about 34% more time) to reach steady state. According to the analysis in Section III, the system with SM controller will expectedly

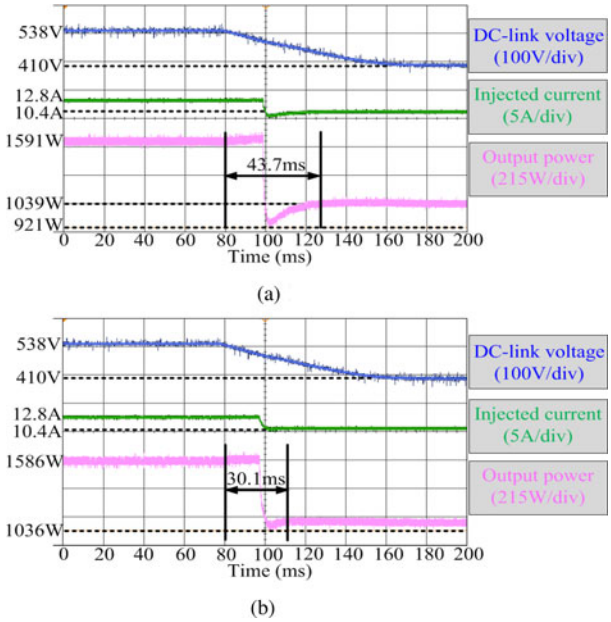

Fig. 37. Experimental results of the dc-link voltage, injected current, and output power of the whole system corresponding to the wind speed changing from 7.9 to 6.6 m/s under (a) PI control and (b) SM control.

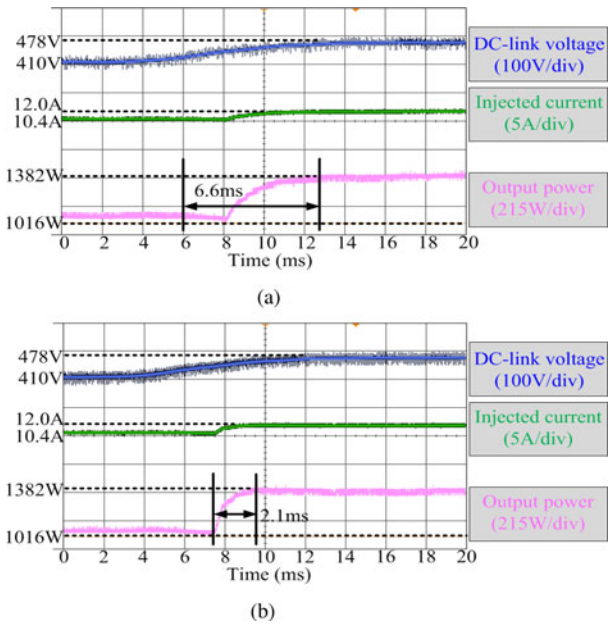

Fig. 38. Experimental results of the dc-link voltage, injected current, and output power of the whole system corresponding to the wind speed changing from 6.6 to 7.3 m/s under (a) PI control and (b) SM control.

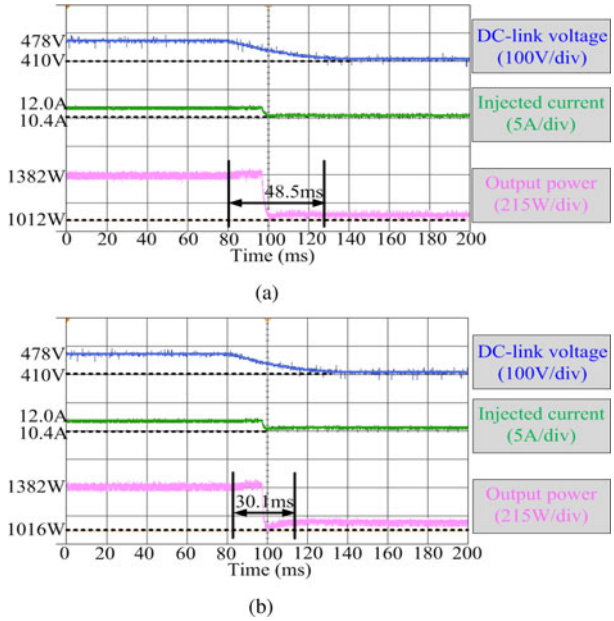

Fig. 39. Experimental results of the dc-link voltage, injected current, and output power of the whole system corresponding to the wind speed changing from 7.3 to 6.6 m/s under (a) PI control and (b) SM control.

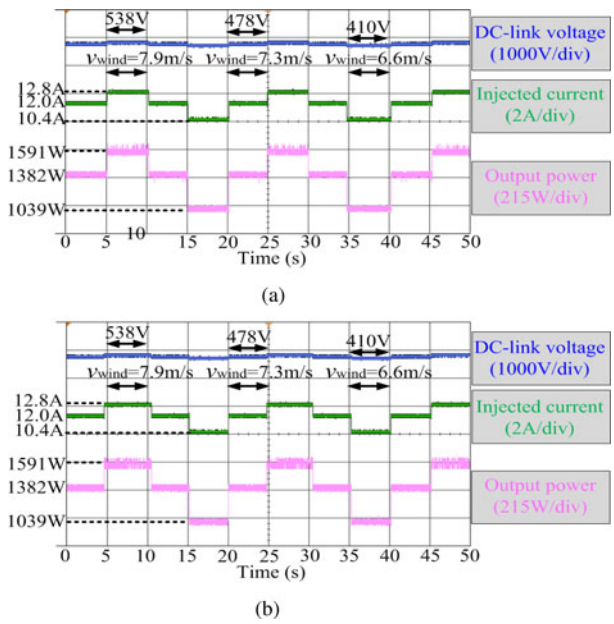

Fig. 40. Experimental results of the dc-link voltage, injected current, and output power of the whole system corresponding to the multiple wind speed change under (a) PI control and (b) SM control.

harvest more energy than that of PI controller. The results in Fig. 36(a) and (b) is in agreement with the simulation results that with the same performance individually for the MPG and MPI, when connected as a system, the SM controller always have better performance than the PI controller. This validates the fact that robustness of the SM controller is better than those of linear controllers.

Various experiments are then performed with the wind speed being changed from 1) 7.9 to 6.6 m/s, 2) 6.6 to 7.3 m/s, and 3) 7.3 to 6.6 m/s. The corresponding results are presented in Figs. 37–39. From the results, the conclusion that the WECS with SM control can harvest more energy can be drawn again as the output power of the SM controller is larger than that of the PI controller.

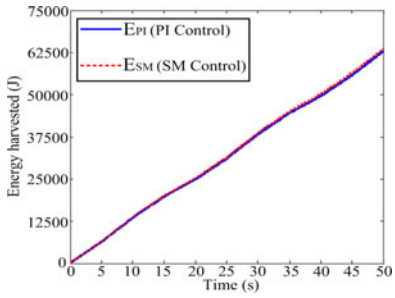

Fig. 41. Energy harvested by SM control (E_{SM}) and PI control (E_{PI}) for the overall system.

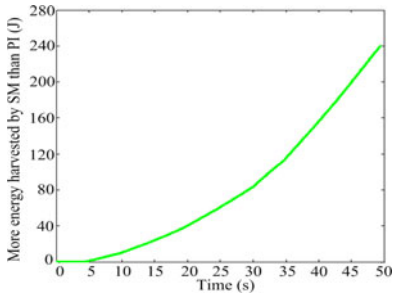

Fig. 42. Additional energy harvested from the wind by SM control than PI control.

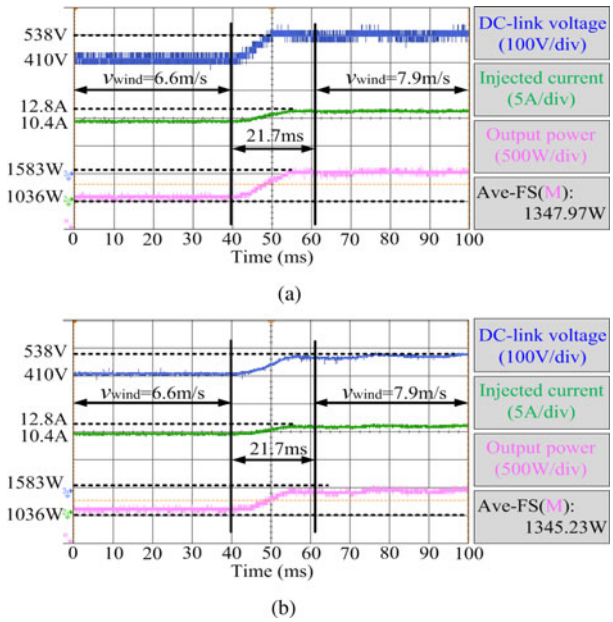

Fig. 43. Experimental results of the dc-link voltage, injected current, and output power of the whole system corresponding to the wind speed changing from 6.6 to 7.9 m/s over a time period of 21.7 ms under (a) PI control and (b) SM control.

Apparently, if the wind speed changes more frequently, the difference in energy harvested by the SM controller and the PI controller is more obvious. Multiple step changes of wind speed from 7.3 m/s to 7.9 m/s to 7.3 m/s to 6.6 m/s to 7.3 m/s to 7.9 m/s to 7.3 m/s to 6.6 m/s to 7.3 m/s to 7.9 m/s, over 50 s, have been evaluated. Results for both the SM and PI controllers are given in Fig. 40. The measured output power over

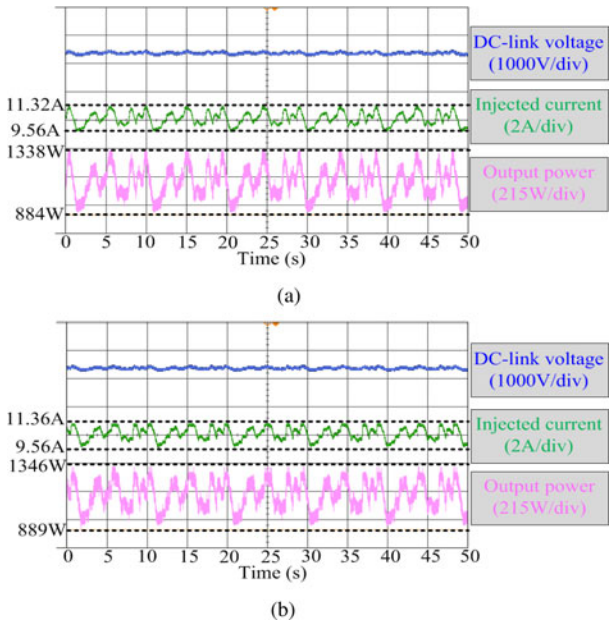

Fig. 44. Experimental results of the dc-link voltage, injected current, and output power of the whole system corresponding to a random wind profile under (a) PI control and (b) SM control.

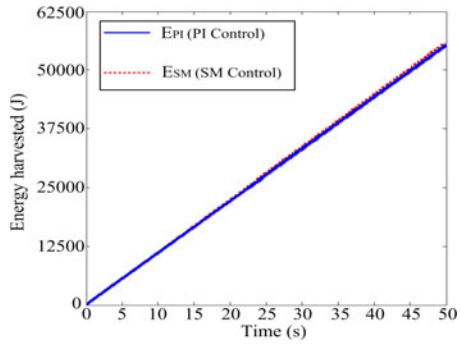

Fig. 45. Energy harvested by SM control (E_{SM}) and PI control (E_{PI}) for the overall system with real-world wind profile.

50 s is time integrated using a MATLAB program to calculate the accumulated energy. Comparisons of the energy harvested are depicted in Fig. 41. The additional energy extracted by the SM controller over the PI control over 50 s is plotted in Fig. 42. For this multiple-step-change test, an improvement of energy harvesting of 0.38% has been recorded, even though the wind speed range is small. Next, the experiment is performed with consideration that the wind velocity may take at least 100 ms to change from 6 to 12 m/s. In our system, the wind velocity are emulated from 6.6 to 7.9 m/s, which means that it will take nearly 20 ms for wind to change from 6.6 to 7.9 m/s. Considering this factor, experimental results for both the SM and PI controllers are given in Fig. 43. From the results, 0.2% more energy can be harvested with the SM controller than the PI controller. Experiments are also conducted with a more random wind profile within the limited wind speed range between 6.6 m/s and 7.9 m/s, as shown in Fig. 44. Comparisons of the

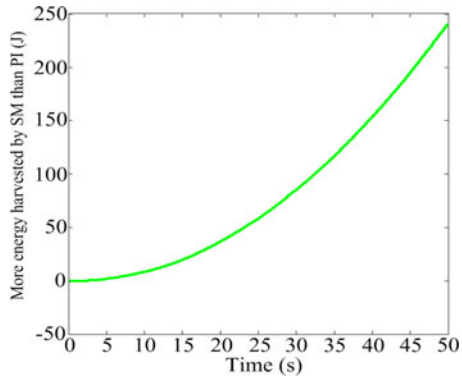

Fig. 46. Additional energy harvested from the wind by SM control than PI control with real-world wind profile.

energy harvested over 50 s with the SM controller and that of the PI controller are provided in Fig. 45. As shown in Fig. 46, 0.44% more energy can be harvested with the SM controller.

VII. Conclusion

In this paper, a low-power wind energy conversion system with variable structure control is proposed for dc grids. To illustrate the capability of this nonlinear controller, a comparison of the system in harvesting wind power with the linear PI controller is performed. Results show that the SM controller has a better transient tracking ability than a PI controller. The SM controller also show its robustness in maximizing power transfer from wind energy to the grid current injection. Overall, the SM controller allows more power to be extracted from the wind in the dynamical scenario than the PI controller. The essence of this paper is to pinpoint that extra energy can be harvested through better dynamical tracking of the wind simply by modifying the control mentioned without altering the hardware of the system.

References

[1] S. M. Muyeen, R. Takahashi, T. Murata, and J. Tamura, "Integration of an energy capacitor system with a variable-speed wind generator," *IEEE Trans. Energy Convers.*, vol. 24, no. 3, pp. 740–749, Sept. 2009.

[2] M. Black and G. Strbac, "Value of bulk energy storage for managing wind power fluctuations," *IEEE Trans. Energy Convers.*, vol. 22, no. 1, pp. 197–205, Mar. 2007.

[3] D. D. Banham-Hall, G. A. Taylor, C. A. Smith, and M. R. Irving, "Flow batteries for enhancing wind power integration," *IEEE Trans. Power Syst.*, vol. 27, no. 3, pp. 1690–1697, Aug. 2012.

[4] J. Wang, D. Xu, B. Wu, and Z. Luo, "A low-cost rectifier topology for variable-speed high-power PMSG wind turbines," *IEEE Trans. Power Electron.*, vol. 26, no. 8, pp. 2192–2200, Aug. 2011.

[5] S. Alepuz, A. Calle, S. Busquets-Monge, S. Kouro, and B. Wu, "Use of stored energy in PMSG rotor inertia for low-voltage ride-through in back-to-back NPC converter-based wind power systems," *IEEE Trans. Ind. Electron.*, vol. 60, no. 5, pp. 1787–1796, May 2013.

[6] I. Munteanu, N. A. Cutululis, A. I. Bratcu, and E. Ceanga, *Optimal Control of Wind Energy Systems : Towards a Global Approach*. New York, NY, USA: Springer, 2008.

[7] N. A. Orlando, M. Liserre, R. A. Mastromauro, and A. Aquila, "A survey of control issues in PMSG-based small wind-turbine systems," *IEEE Trans. Ind. Informat.*, vol. 9, no. 3, pp. 1211–1221, Aug. 2013.

[8] Y. Wang, D. Panda, T. A. Lipo, and P. Di, "Open-winding power conversion systems fed by half-controlled converters," *IEEE Trans. Power Electron.*, vol. 28, no. 5, pp. 2427–2436, May 2013.

[9] D. Battista, P. F. Puleston, R. J. Mantz, and C. F. Christiansen, "Sliding mode control of wind energy systems with DOIG-power efficiency and torsional dynamics optimization," *IEEE Power Syst.*, vol. 15, no. 2, pp. 728–734, May 2000.

[10] B. G. Rawn, P. W. Lehn, and M. Maggiore, "Control methodology to mitigate the grid impact of wind turbines," *IEEE Trans. Energy Convers.*, vol. 22, no. 2, pp. 431–438, Jun. 2007.

[11] K. Y. Lo, Y. M. Chen, and Y. R. Chang, "MPPT battery charger for stand-alone wind power system," *IEEE Trans. Power Electron.*, vol. 26, no. 6, pp. 1631–1638, Jun. 2011.

[12] P. Wang, Z. Gao, and L. Bertling, "Operational adequacy studies of power systems with wind farms and energy storages," *IEEE Power Syst.*, vol. 27, no. 4, pp. 2377–2384, Nov. 2012.

[13] Y. K. Tan and S. K. Panda, "Optimized wind energy harvesting system using resistance emulator and active rectifier for wireless sensor nodes," *IEEE Trans. Power Electron.*, vol. 26, no. 1, pp. 38–50, Jan. 2011.

[14] Y. Tang and L. Xu, "A flexible active and reactive power control strategy for a variable speed constant frequency generating system," *IEEE Trans. Power Electron.*, vol. 10, no. 4, pp. 472–478, Jul. 1995.

[15] Y. Juan, "An integrated-controlled AC/DC interface for microscale wind power generation systems," *IEEE Trans. Power Electron.*, vol. 26, no. 5, pp. 1377–1384, May 2011.

[16] V. Kumar, R. R. Joshi, and R. C. Bansal, "Optimal control of matrix-converter-based WECS for performance enhancement and efficiency optimization," *IEEE Power Syst.*, vol. 27, no. 4, pp. 2377–2384, Nov. 2012.

[17] Y. Xia, K. H. Ahmed, and B. W. Williams, "A new maximum power point tracking technique for permanent magnet synchronous generator based wind energy conversion system," *IEEE Trans. Power Electron.*, vol. 26, no. 12, pp. 3609–3620, Dec. 2011.

[18] S. M. R. Kazmi, H. Goto, H. J. Guo, and O. Ichinokura, "A novel algorithm for fast and efficient speed-sensorless maximum power point tracking in wind energy conversion system," *IEEE Trans. Ind. Electron.*, vol. 58, no. 1, pp. 29–36, Jan. 2011.

[19] C. T. Pan and Y. L. Juan, "A novel sensorless MPPT controller for a high-efficiency microscale wind power generation system," *IEEE Trans. Energy Convers.*, vol. 25, no. 1, pp. 207–216, Mar. 2010.

[20] R. M. Hilloowala and A. M. Sharaf, "A utility interactive wind energy conversion scheme with an asynchronous DC link using a supplementary control loop," *IEEE Trans. Energy Convers.*, vol. 9, no. 3, pp. 558–563, Sep. 1994.

[21] I. Tsoumas, A. Safacas, E. Tsimplostefanakis, and E. Tatakis, "An optimal control strategy of a variable speed wind energy conversion system," *IEEE Trans. Energy Convers.*, vol. 9, no. 3, pp. 558–563, Sep. 1994.

[22] R. Datta and V. T. Ranganathan, "A method of tracking the peak power points for a variable speed wind energy conversion system," *IEEE Trans. Energy Convers.*, vol. 18, no. 1, pp. 163–168, Mar. 2003.

[23] K. Tan and S. Islam, "Optimum control strategies in energy conversion of PMSG wind turbine system without mechanical sensors," *IEEE Trans. Energy Convers.*, vol. 19, no. 2, pp. 392–399, Jun. 2004.

[24] Q. Wang and L. Chang, "An intelligent maximum power extraction algorithm for inverter-based variable speed wind turbine systems," *IEEE Trans. Power Electron.*, vol. 19, no. 5, pp. 1242–1249, Sep. 2004.

[25] B. Beltran, T. Ahmed-Ali, and M. E. H. Benbouzid, "Sliding mode power control of variable-speed wind energy conversion systems," *IEEE Trans. Energy Convers.*, vol. 23, no. 2, pp. 551–558, Jun. 2008.

[26] H. De Battista, R. J. Mantz, and C. F. Christiansen, "Dynamical sliding mode power control of wind driven induction generators," *IEEE Trans. Energy Convers.*, vol. 15, no. 4, pp. 451–457, Dec. 2000.

[27] B. Beltran, T. Ahmed-Ali, and M. Benbouzid, "High-order sliding-mode control of variable-speed wind turbines," *IEEE Trans. Ind. Electron.*, vol. 56, no. 9, pp. 3314–3321, Sep. 2009.

[28] Y. Xia, K. H. Ahmed, and B. W. Williams, "Wind turbine power coefficient analysis of a new maximum power point tracking technique," *IEEE Trans. Ind. Electron.*, vol. 60, no. 3, pp. 1122–1132, Mar. 2013.

[29] Z. M. Dalala, Z. U. Zahid, and J. S. Lai, "New overall control strategy for small-scale WECS in MPPT and stall regions with mode transfer control," *IEEE Trans. Energy Convers.*, vol. 28, no. 4, pp. 1082–1092, Dec. 2013.

[30] Z. M. Dalala, Z. U. Zahid, W. Yu, and Y. Cho, "Design and analysis of an MPPT technique for small-scale wind energy conversion systems," *IEEE Trans. Energy Convers.*, vol. 28, no. 3, pp. 756–767, Sep. 2013.
[31] V. Akhmatov, "Variable-speed wind turbines with doubly-fed induction generators. Part IV: Uninterrupted operation features at grid faults with converter control coordination," *Wind Eng.*, vol. 26, no. 2, pp. 519–529, Jul. 2009.
[32] S. Heier, *Grid Integration of Wind Energy Conversion Systems*. New York, NY, USA: Wiley, 1998.
[33] V. I. Utkin, "Sliding mode control design. principles and applications to electric drives," *IEEE Trans. Ind. Electron.*, vol. 40, no. 1, pp. 23–36, Jan. 1993.
[34] S. C. Tan, Y. M. Lai, and C. K. Tse, *Sliding Mode Control of Switching Power Converters - Techniques and Implementation*. Boca Raton, FL, USA: CRC, 2012.

Yun Yang (S'13) was born in Hangzhou, China. He received the B.S. degree from Wuhan University, Wuhan, China, in 2012. He is currently working toward the Ph.D. degree in Power Electronics Research Group, Department of Electrical and Electronic Engineering, The University of Hong Kong, Hong Kong.

He is the member of Mensa, Hong Kong Section. His current research interests include variable structure control and predictive control of power electronics.

Kwan-Tat Mok (S'14) received the B.Eng. and M.Phil. degrees in electronic and information engineering from the Hong Kong Polytechnic University, Kowloon, Hong Kong, in 2009 and 2012. He is currently working toward the Ph.D. degree in Power Electronics Research Group, Department of Electrical and Electronic Engineering, The University of Hong Kong, Hong Kong.

In 2007, he worked as an Engineering Trainee in Solomon Systech Limited, Hong Kong, for a one-year internship program. His research interests include smart grid technology, electric springs and electronic drivers for light-emitting diodes.

Siew-Chong Tan (S'00–M'06–SM'11) received the B.Eng. (Hons.) and M.Eng. degrees in electrical and computer engineering from the National University of Singapore, Singapore, in 2000 and 2002, respectively, and the Ph.D. degree in electronic and information engineering from the Hong Kong Polytechnic University, Hong Kong, in 2005.

From October 2005 to May 2012, he worked as a Research Associate, Postdoctoral Fellow, Lecturer, and Assistant Professor in the Department of Electronic and Information Engineering, Hong Kong Polytechnic University. From January to October 2011, he was a Senior Scientist in Agency for Science, Technology and Research (A*Star), Singapore. He is currently an Associate Professor in the Department of Electrical and Electronic Engineering, The University of Hong Kong, Hong Kong. He was a Visiting Scholar at the Grainger Center for Electric Machinery and Electromechanics, University of Illinois at Urbana-Champaign, Champaign, IL, USA, from September to October 2009, and an Invited Academic Visitor of Huazhong University of Science and Technology, Wuhan, China, in December 2011. He is a coauthor of the book *Sliding Mode Control of Switching Power Converters: Techniques and Implementation* (Boca Raton, FL, USA: CRC, 2011). His research interests include the areas of power electronics and control, LED lightings, smart grids, and clean energy technologies. Dr. Tan serves extensively as a Reviewer for various IEEE/IET transactions and journals on power, electronics, circuits, and control engineering.

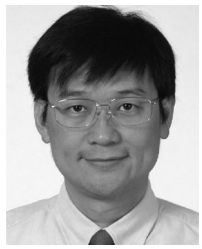

S. Y. (Ron) Hui (M'87–SM'94–F'03) received the B.Sc. Eng. (Hons.) degree from the University of Birmingham, Birmingham, U.K., in 1984, and the D.I.C. and Ph.D. degrees from Imperial College London, London, U.K., in 1987.

He is currently the Philip Wong Wilson Wong Chair Professor at the University of Hong Kong, Hong Kong and a Chair Professor at Imperial College London. He has published more than 300 technical papers, including more than 180 refereed journal publications. More than 55 of his patents have been adopted by industry.

Dr. Hui is an Associate Editor of the IEEE TRANSACTIONS ON POWER ELECTRONICS and the IEEE TRANSACTIONS ON INDUSTRIAL ELECTRONICS, and an Editor of the IEEE JOURNAL OF EMERGING AND SELECTED TOPICS IN POWER ELECTRONICS. He was appointed twice as an IEEE Distinguished Lecturer by the IEEE Power Electronics Society in 2004 and 2006, he received the IEEE Best Paper Award from the IEEE IAS in 2002, and two IEEE Power Electronics Transactions Prize Paper Awards in 2009 and 2010. His inventions on wireless charging platform technology underpin key dimensions of Qi, the world's first wireless power standard, with freedom of positioning and localized charging features for wireless charging of consumer electronics. In Nov. 2010, he received the IEEE Rudolf Chope R&D Award from the IEEE Industrial Electronics Society and the IET Achievement Medal (The Crompton Medal). He is a Fellow of the Australian Academy of Technological Sciences & Engineering and received the 2015 IEEE William E. Newell Power Electronics Award.